Tellus SERIES B CHEMICAL AND PHYSICAL METEOROLOGY
PUBLISHED BY THE INTERNATIONAL METEOROLOGICAL INSTITUTE IN STOCKHOLM

Tellus (2010), 62B, 69–86
Printed in Singapore. All rights reserved

TELLUS

Investigation of aerosol–cloud interactions using a chemical transport model constrained by satellite observations

By YAN FENG* and V. RAMANATHAN, *Center for Atmospheric Sciences, Scripps Institution of Oceanography, University of California, San Diego, La Jolla, CA 92093-0221, USA*

(Manuscript received 10 February 2009; in final form 11 September 2009)

ABSTRACT

This study simulates optical depth of marine warm clouds for year 2001 based on interactively predicted aerosol concentrations with a global chemical transport model (CTM) driven by the ERA-40 re-analysis meteorological data. The simulated aerosol and cloud droplet number concentrations (CDNC) largely reproduce the variations between polluted and pristine marine environment as revealed by surface and aircraft measurements. By constraining cloud liquid water path (CLWP) with satellite microwave measurements, the simulated global and southern hemispheric aerosol optical depth (AOD) and cloud optical depth (COD) are well within 10% of the observed values. As a result of larger anthropogenic aerosol loadings over the northern oceans, the simulated CDNC and COD are, respectively, by 51 and 18% higher than those over the southern oceans, while the column-averaged droplet effective radius is 13% smaller. These simulated interhemispheric differences, while qualitatively consistent with satellite observations, are larger than the observations. Inclusion of drizzle effect improved the disparities but not entirely. The constrained CTM generally captures the seasonality in AOD and CLWP observations, and demonstrates that annual cycle of COD is dominated by CLWP. During winter monsoon the simulated and observed COD correlate more strongly with changes in AOD over the N. Indian Ocean.

1. Introduction

The critical role of aerosols in the determination of cloud radiative properties is far from being accurately evaluated on a global basis, largely because aerosol–cloud interactions are manifested in both cloud macro- and microphysical properties. With constant liquid water content, an increase in aerosol number concentration can lead to an increase in cloud droplet number concentrations (CDNC) and a reduction in droplet size, followed by an enhancement in cloud optical depth (COD) and albedo. This is the so-called Twomey's or cloud albedo effect (Twomey, 1974). Aerosols serving as cloud condensation nuclei (CCN) could also increase cloud cover and height, and suppress the onset of precipitation. These effects are referred as cloud lifetime effect (Albrecht, 1989), and often considered in climate feedbacks. Many observational evidences established the links between the atmospheric abundance of aerosols to the changes of cloud properties (Conover, 1966; Coakley et al., 1987; Kaufman and Nakajima, 1993; Han et al., 1994; Reid et al., 1999; Andreae et al., 2004). However, estimates of the aerosol effects by global modelling or remote sensing alone have considerable discrepancies, subject to individual uncertainties and limitations (Forster et al., 2007). Satellite-based estimate of the cloud albedo effect due to aerosols is about -0.2 ± 0.1 Wm^{-2} (Quaas et al., 2008). And it is much smaller than the IPCC-reported median value of -0.7 Wm^{-2} with a 5–95% range of -0.3 to -1.8 Wm^{-2}, based on chemical transport or global climate model simulations (Forster et al., 2007).

The fundamental difficulty in judging the validity of global model simulations of aerosol–cloud interactions is the lack of such reliable global data sets that can be directly used to evaluate the simulated aerosol and cloud microphysical parameters at both fine time resolution and large spatial scale. Physically based parametrizations, which were developed to account for the microphysical processes between aerosol particles and cloud droplets in large-scale models (Twomey, 1959; Ghan et al., 1993; Chuang and Penner, 1995; Ghan et al., 1995; Abdul-Razzak et al., 1998; Abdul-Razzak and Ghan, 2000, 2002; Nenes and Seinfeld, 2003), have often been evaluated in the campaign-based closure studies (Lance et al., 2004). However, the performance of these parametrizations rely greatly on the input parameters, thus is often limited by the predicted aerosol

*Corresponding author.
e-mail: yafeng@ucsd.edu
DOI: 10.1111/j.1600-0889.2009.00444.x

concentrations, size distribution, chemical composition, mixing state, as well as the in-cloud updraft velocities, ambient temperature and moisture supply from location to location. Lohmann and Feichter (2005) suggests that connecting aerosol particles to cloud droplets on a global scale is probably still the weakest point in the estimation of indirect aerosol effects with global climate models.

Optical depth of clouds retrieved by satellite visible radiometers provides temporal and spatial distributions of the cloud characteristics with reasonably good quality, that is, uncertainty in the MODIS-retrieved COD is about 21% compared with surface measurements (Minnis et al., 2004). More importantly, evaluation of the simulated COD, instead of radiation fluxes, will not be affected by significant uncertainties associated with cloud cover generated by climate models. However, COD depends on not only cloud microphysical properties, but also the amount of condensed water in the form of clouds. Cloud liquid water path (CLWP), which is the vertical integral of liquid water content in cloud, varies significantly between models, re-analysis data and satellite observations (Li et al., 2008). Conceptually, CLWP is predominantly determined by the convergence of moisture into forming clouds, which is driven by dynamical processes on the cloud- to meso- to synopticscales. Aerosol effects, that is, by changing the on-set of precipitation processes (Ackerman et al., 2004) or the vertical extension of cloud height (Andreae et al., 2004), are generally considered to be secondary. With this assumption, if CLWP is constrained from observations, then a comparison of the simulated and satellite-derived COD may yield much needed insights into the aerosol cloud albedo effect. The validity of this approach hinges on choosing independent measurements for CLWP and COD. It is mainly for this reason that the satellite-based microwave radiometer data are selected for CLWP and the visible radiometer data are used for COD in this study. In addition, microwave measurements of CLWP are less susceptible to errors from contamination of broken clouds, and can retrieve a wide range of values without saturating or requiring additional information on the cloud droplet size, compared to the visible/infrared-band measurements (Turner et al., 2007).

A few studies attempted to combine chemical transport model (CTM) simulations with satellite-based cloud observations directly in the investigation of aerosol–cloud interactions. Using a CTM, Schwartz et al. (2002) conducted a study on the simulated sulphate loadings in comparison with the differences in the observed cloud properties. By mapping out the dependencies of COD on CLWP (under the same CLWP conditions), they showed the median cloud-top albedo was enhanced by 0.02–0.15 during two pollution episodes over the North Atlantic in April, 1997. Chameides et al. (2002) correlated the model-simulated anthropogenic aerosol burdens with the International Satellite Cloud Climatology Project (ISCCP) COD products, and found good consistency in the geographical distribution of aerosol and cloud properties in East Asia.

This study investigates the role of aerosols in optical depth of marine warm clouds, by using a global CTM implemented with a warm cloud microphysics scheme to calculate CDNC based on simulated aerosol concentrations, and using the satellite-constrained CLWP as an input to calculate COD and cloud droplet effective radius (CDR). Comparison with satellite observations of cloud optical properties (COD and CDR) would then allow us to examine the simulated aerosol effects in the spatial and temporal variations of these cloud fields. Global model simulations can also distinguish the relative contribution by anthropogenic components from natural aerosols to the observed cloud optical properties. Furthermore, the influence of atmospheric dynamics has been captured by the observation-constrained CLWP presumably. So it is most likely that the deficiencies in the simulated cloud optical fields would mainly arise from the simulated aerosol–cloud interactions and the input aerosol properties. To further isolate the impact of simulated aerosol–cloud interactions, we evaluate the aerosol properties simulated by the model with the ground-based and in situ aircraft measurements as well as satellite observations. We hope to provide valuable information for future improvement of aerosol treatment in the integrated climate models by identifying deficiencies in simulations of COD. This study focuses on marine warm clouds, which are major contributors to the cloud radiative forcing for their extensive coverage (Ramanathan et al., 1989; Harrison et al., 1990), but their radiative effects are poorly represented in global climate models (Zhang et al., 2005).

The global CTM and the satellite-based cloud data sets used in this study are described in Section 2. Section 3 examines the predicted aerosol and cloud droplet concentrations in comparison with the ground-based and aircraft measurements. The simulated aerosol and marine warm CODs are presented and discussed with satellite observations in Section 4. Regional analyses of the aerosol–cloud interactions in the subtropical marine stratus/stratocumulus clouds are discussed in the Section 5. Finally, Section 6 summarizes the major results of this study.

2. Methodology

2.1. Global chemical transport model

The CTM is modified from the University of Michigan version of the Lawrence Livermore National Laboratory (Umich/LLNL) IMPACT model (Liu and Penner, 2002; Feng et al., 2004; Rotman et al., 2004; Liu et al., 2005; Feng and Penner, 2007). The model resolution is 2° latitude by 2.5° longitude in the horizontal, with 26 vertical layers from the surface to 0.1 hPa. For this study, the CTM is driven by the European Centre for Medium-Range Weather Forecasts (ECMWF) 40-yr re-analysis (ERA-40) meteorological data fields (Uppala et al., 2005) for year 2001, which are available at 6-h time intervals and interpolated to the model 1-h time step for tracer advection. The transport and deposition schemes is fully described in Rotman

et al. (2004) for the original IMPACT model. A short version is given Section A.1 of the Appendix.

Sea salt and mineral dust aerosols are considered in four size bins (radius: <0.63, 0.63–1.26, 1.26–2.5 and 2.5–10 μm), while sulphate and carbonaceous aerosols are treated in three size bins (radius: <0.05, 0.05–0.63 and 0.63–1.26 μm) and one size bin (radius: <0.63 μm), respectively. The concentrations of SO_2, SO_4^{2-}, H_2O_2 and DMS are simulated with an online sulfur model (Liu and Penner, 2002; Liu et al., 2005), including emissions of SO_2 from fossil fuel burning of 68.9 Tg-S yr^{-1} (Nakicenovic et al., 2000), non-eruptive volcanoes of 4.8 Tg-S yr^{-1} (Andres and Kasgnoc, 1998) and an oceanic DMS source of 26 Tg-S yr^{-1} (Kettle and Andreae, 2000). SO_2 is oxidized to SO_4^{2-} in cloud by the dissolved O_3 and H_2O_2, and in the gas phase by the OH radical. Both OH and NO_3 radicals oxidize DMS and generate SO_4^{2-}. The size-segregated sea salt mass fluxes are calculated online based on the algorithm given by Monahan et al. (1986), depending on the interpolated hourly 10-m wind speed from the ERA-40 re-analysis data (details given in Section A.1). The hygroscopic growth of sulphate and sea salt aerosols in dry deposition is accounted for using the empirical expression of Gerber (1985).

In addition to sulphate and sea salt, global distributions of other aerosol concentrations including dust, black carbon and organic carbon aerosols are also simulated for aerosol optical depth (AOD). Dust and black carbons aerosols may become hygroscopic during their aging in the atmosphere. But they are not considered as CCN in this study, since the mixing of those aerosols with soluble substances in the atmosphere are still quite uncertain. Similar difficulty exists for the global model representation of hygroscopicity of organic aerosols, which is mainly limited by the knowledge on the formation of secondary organic aerosols. The omission of these aerosol types in cloud microphysics are assumed not to impose significant errors in model simulations of marine warm clouds, because their concentrations are relatively low over the oceans, compared to sulphate and sea salt aerosols. Detailed descriptions of the aerosol module in the CTM are given in Liu et al. (2005) and Feng and Penner (2007). The annual mean aerosol burdens and optical depth (at 550 nm) calculated by the global model are summarized in Table 1 for the simulated year 2001. They are generally in the ranges of other model predictions in literature (Kinne et al., 2006). Further comparison of the fine-mode AOD (by submicron particles) with satellite observations will be discussed in Section 4.

2.2. *Cloud microphysics*

A cloud microphysics scheme is developed to obtain CDNC for warm clouds over the oceans. Details are provided in Section A.2 of the Appendix. In brief, aerosol activation spectrum (CCN as

Table 1. Comparison of annual mean aerosol burden and optical depth at 550nm of the model simulations (for year 2001) with the median, minimum and maximum of 16 models from AeroCom (for year 2000) (Kinne et al., 2006)

	Model	AeroComMedian	AeroCom Minimum	AeroCom Maximum
Aerosol burden (mg m^{-2})				
Sulphate	4.2	3.9	1.8	5.3
POM	3.0	3.3	0.9	5.0
BC	0.38	0.39	0.09	1.0
Dust	33.8	39.1	8.8	57.8
Sea salt	13.0	12.6	4.8	25.8
Aerosol optical depth at 550 nm[a]				
Sulphate	0.040	0.034	0.015	0.051
POM	0.024	0.019	0.006	0.030
BC	0.004	0.004	0.0017	0.0088
Dust	0.019	0.032	0.012	0.054
Sea salt	0.052	0.030	0.021	0.067
Total	0.138	0.127	0.065	0.151

[a]The hygroscopic growth of sulphate [$(NH_4)_2SO_4$] and sea salt (NaCl) aerosols is calculated with a thermodynamic equilibrium model (EQUISOLV II) (Jacobson, 1999), and the relative humidity dependence for POM follows that in the GOCART model (Chin et al., 2002). At relative humidity 80%, the calculated aerosol extinction coefficient at 550 nm with Mie scattering is 12 m^2 g^{-1} for sulphate, 10 m^2 g^{-1} for POM and for four sea salt aerosol bins: 10, 4, 2 and 1 m^2 g^{-1}, respectively. Dust and BC (black carbon) are assumed to be hydrophobic aerosols. The extinction coefficient of BC at 550 nm is 10 m^2 g^{-1} (Chin et al., 2002). And for four dust aerosol bins, the calculated extinction coefficients are 2.5, 0.8, 0.38 and 0.12 m^2 g^{-1}, respectively.

a function of supersaturation ratio, S) is computed from Köhler theory, as a function of aerosol number concentrations (varying between 10 and 5000 cm^{-3}), and chemical composition in the two size ranges: Aitken (particle diameter, $D_p < 0.1\ \mu m$) and accumulation ($0.1\ \mu m < D_p < 1.25\ \mu m$). By fitting these spectrums to the power-law relationships ($CCN = CS^k$) in segments, CDNC (N_d) and the maximum supersaturation (S_{max}) in ascending can be obtained from analytic solutions by Twomey (1959). Then a smoothed relationship linking N_d to updraft velocity is numerically calculated and used to generate a lookup table for the grid-mean cloud droplet concentration ($\overline{N_d}$) by

$$\begin{cases} \overline{N_d} = \sum_i N_d(W_i) \times f(\omega_i) \\ W_i = \omega_{ls} + \omega_i \end{cases}, \tag{1}$$

where ω_{ls} denotes the large-scale mean vertical velocity in a grid box. $f(\omega_i)$ denotes the subgrid variability of the in-cloud updraft velocity (ω_i), represented by a normalized probability density function (PDF) with a mean velocity of 0.14 ms^{-1} and a standard deviation of 0.11 ms^{-1}. These PDF parameters were the lowest values observed for marine stratocumulus during CSTRIPE (Meskhidze et al., 2005), but gave best estimates in global calculations. Uncertainty associated the subgrid variability of updraft velocity is estimated about ±30% in the obtained droplet concentrations (Meskhidze et al., 2005). For clouds with small cloud fractions (less than 5%), a more convective updraft velocity distribution is used following that observed in trade cumulus during INDOEX (McFarquhar and Heymsfield, 2001). At each time step, CDNC in a single grid box is interpolated from the look-up table, depending on the interactively predicted, that is, aerosol number concentration, fractions of sulphate and sea salt aerosols in the two size ranges, in-cloud updraft velocity and temperature.

Liquid water amount in drizzle drops are often detected by the satellite-based microwave measurements of CLWP, if cloud is drizzling. The cloud–rain threshold used in the SSM/I microwave CLWP data (detailed in the next section) is 2500 gm^{-2}, below which all of the condensed water is designated to cloud droplets. But light drizzle occurs when CLWP is above 180 gm^{-2} (Wentz, 1997). In the visible/near-infrared wavelengths, large-size drizzle drops (>20 μm in radius) are much less reflective compared to smaller cloud droplets (<15 μm). In order to account for the potential radiative effect, a parametrization following the observed relationships between drizzle drop number concentration and the volume-mean cloud droplet size (Pawlowska and Brenguier, 2003) is included. For simplicity, the size of drizzle drops is assumed to be uniformly 35 μm in radius. In the presence of drizzle, the calculated droplet number concentration is also reduced by 37%, which is the removal efficiency due to the coalescence/coagulation between 10-μm cloud droplets and 35-μm drizzle drops (Rogers and Yau, 1999). A maximum volume-mean radius of 10 μm is suggested as the critical size for the drizzle formation based on the in situ aircraft measurements (Pawlowska and Brenguier, 2003). We adopted a smaller size of 7.5 μm in our standard simulations, because the calculated volume-mean radius should represent the average droplet size in cloud and is usually smaller than the maximum value. Sensitivity studies are performed on the selected critical droplet size in Section 5.1.

Optical depth (τ) and effective radius (r_e) of clouds are then calculated by

$$\tau = \tau_{cd} + \tau_{dz} = \int \left(\frac{3LWC_{cd}}{2\rho_w r_e} + 2n_{dz}\pi R_{dz}^2 \right) dz \tag{2}$$

$$r_e = k \left(\frac{3LWC_{cd}}{4\pi\rho_w \overline{N_d}} \right)^{1/3}, \tag{3}$$

where τ_{cd} and τ_{dz} denote the optical depth of cloud droplets and drizzle drops (if present), respectively. ρ_w is the water density ($g\,m^{-3}$). $\overline{N_d}$ is the CDNC, and LWC_{cd} is the liquid water content associated with cloud droplets, which equals to the total LWC minus that in drizzle drops with a number concentration of n_{dz}, and a radius (R_{dz}) of 35 μm. In eq. (3), k is the dispersion coefficient, proportional to the relative dispersion of a cloud droplet size spectrum. An empirical expression of k by fitting multiple in situ aircraft measurements (Liu and Daum, 2002; Rotstayn and Liu, 2003) is included in the CTM. Other observational studies such as Martin et al. (1994), McFarquhar and Heymsfield (2001) and Miles et al. (2000) suggested the similar relationships that pristine clouds tend to have a smaller relative dispersion (thus k) than polluted clouds.

2.3. *Satellite-based cloud liquid water path and optical depth*

In this study, CLWP is originally derived from the ERA-40 meteorological data and then adjusted to the Special Sensor Microwave/Imager (SSM/I) microwave measurements on the monthly mean basis. The satellite-based monthly mean LWP for non-precipitating water clouds is calculated from the 0.25° × 0.25° SSM/I daily data (version 6) aboard the DMSP-F14, provided by Remote Sensing Systems (RSS). The SSM/I instrument measures the grid-mean liquid water path, and could underestimate for partially cloudy grids. This bias is considered small, as the studied marine stratiform clouds usually have cloud fractions larger than 1.25% of a global model grid (2° × 2.5°), about the same size as a single SSM/I grid cell. The NASA MODIS/Terra edition 5 level-3 (1° × 1°) daily cloud fractions for liquid water clouds (Platnick et al., 2003) are used as weighting functions in aggregating the 0.25° data to the global model grids, and also in time averaging. The MODIS/Terra cloud optical properties derived from the visible/near-infrared reflectance measurements are available at an approximate equator-crossing time of 10:30 am. Accordingly, the SSM/I morning-pass data, which pass overhead at equator around 8:28 am, is used to constrain the monthly mean daytime CLWP calculated from the 6-hourly ERA40 data

within the local time from 6 am to 12 am. To be comparable with the MODIS/Terra daytime cloud retrievals, the CTM simulates cloud optical properties at local time between 9:30 am and 11:30 am, with the interpolated CLWP at 1-h intervals. This time interpolation of CLWP results in small discrepancies between the constrained CLWP and the SSM/data; on a monthly basis, the percent error is estimated within 1%.

Figure 1 shows the extracted monthly mean CLWP over the global model domain ($2^\circ \times 2.5^\circ$) in July, before (original ERA-40 data) and after constrained with the SSM/I microwave data. After the adjustment, the absolute amount of the condensed water in clouds from the original ERA-40 data set is significantly reduced, especially in the mid- and high- latitudes. The overestimation in CLWP generated by large-scale climate models seems to be a more common problem, as Li et al. (2008) has shown that multiple GCMs tend to predict much larger CLWPs than the satellite liquid water estimates (MODIS, SSM/I, ISCCP and CloudSat). Without constraining the CLWP, the estimate of aerosol cloud albedo effect by global climate models are likely to be overpredicted.

The daily CLWPs are obtained by scaling the SSM/I monthly mean data with the temporal profiles derived from the ERA-40 cloud fields as well as the vertical distributions. The long-operating satellite radiation instruments in both visible and microwave bands have difficulties of yielding the robust vertical information in clouds. This situation could improve in future after launches of the CALIPSO and CloudSat satellites. Meanwhile, liquid water vertical profiles generated by the ECMWF model (by which the ERA-40 re-analyses data is generated) have been evaluated through systematic comparisons and performed reasonably well (Illingworth et al., 2007). As for the daily variability of CLWP, the satellite-based SSM/I daily measurements are not available for every grid cell in the global domain, as their retrievals are limited by rain contamination, spatial coverage at low latitudes, and missing data. For example, only about half of the model grids over the ocean have utilizable daily CLWP data for more than 15 d in July 2001. More importantly, constraining the monthly mean allows for the cloud fields to still be consistent in the CTM. The daily variability of CLWP used in the simulations is examined against with the satellite observations in Section 5.1.

Monthly and daily MODIS aerosol and cloud products: MOD08_M3 and MOD08_D3 (edition 5; Platnick et al., 2003) are used in global and regional analyses. Both of them are quality-assured level-3 products, available at $1^\circ \times 1^\circ$ grids for the simulated time period of year 2001. The gridded satellite data are downscaled to the CTM grid size of $2^\circ \times 2.5^\circ$, weighted by their correspondingly retrieved cloud fractions. Randomly overlapping scheme is assumed in the CLWP and COD calculations. The resulting annual mean cloud fractions for marine warm clouds (below 500 hPa) based on the ERA-40 data are about 40–60% in subtropics and as much as 60–80% in extra-tropics, consistent with the MODIS cloud fractions (MOD08_M3) averaged for combined-phase and liquid water clouds.

Figure 2 shows a schematic illustration of the incorporation of the cloud microphysics parametrization described in Section 2.2 and the satellite-based CLWP into the global aerosol and chemistry transport model. The integrated model was run for 12 months of the year 2001. A 2-month spin-up time for January was used to generate background values as initial concentrations for the production runs. The global model requires ∼1 h of CPU time on 16 IBM SP5 processors to complete a 1-month simulation.

3. Evaluation of simulated aerosols and clouds with *in situ* observations

Figure 3 compares the simulated daily mean aerosol number concentrations (cm^{-3}) with surface measurements at the Atmospheric Brown Clouds (ABC) observatories located over the N.

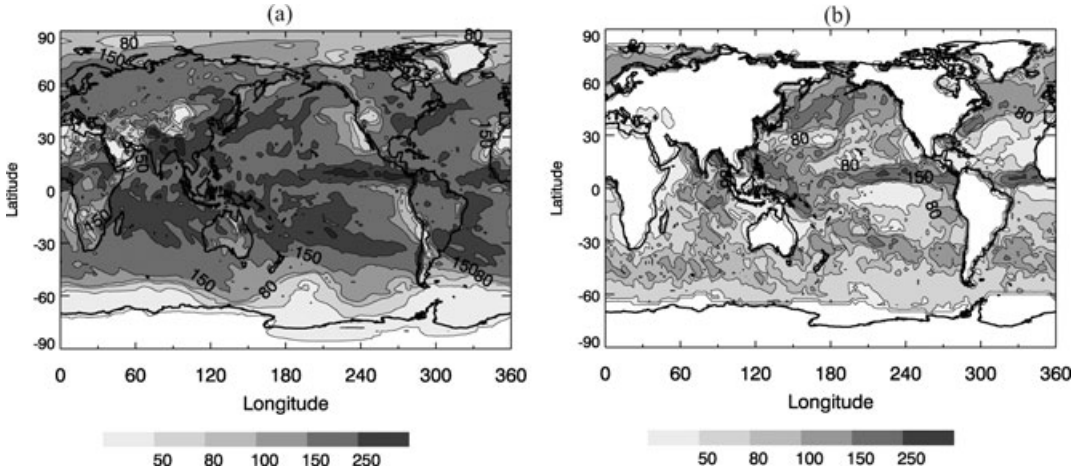

Fig. 1. The monthly mean cloud liquid water path ($g\,m^{-2}$) in July 2001, (a) from the ERA-40 meteorological data set and (b) in the CTM simulations after constrained by the SSM/I microwave measurements.

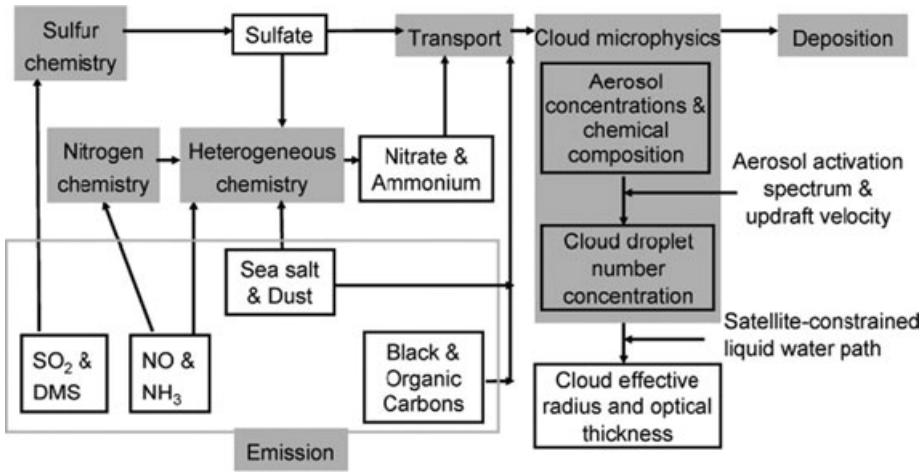

Fig. 2. The schematic of the global chemical transport model (CTM).

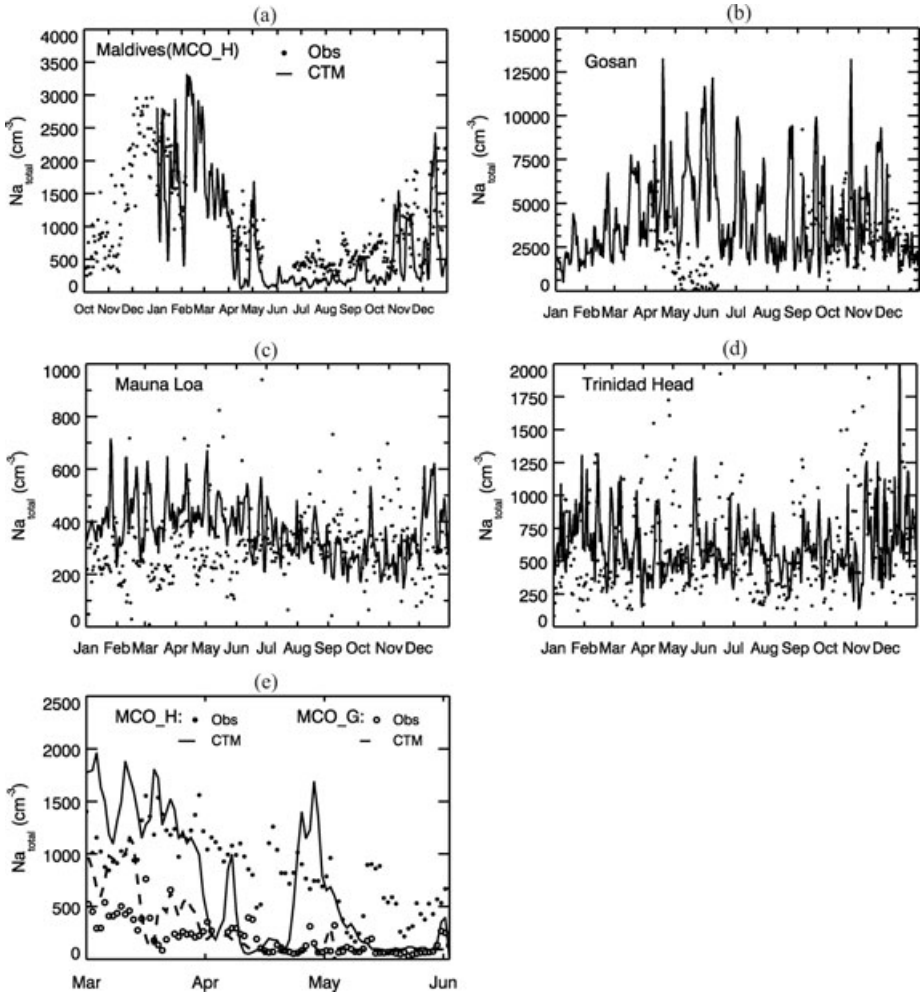

Fig. 3. Comparison of daily mean aerosol number concentration between the CTM simulations and surface measurements (Obs) at the ABC observatories: (a) Maldives (2004–2005), (b) Gosan (2001), (c) Mauna Loa (2001) and (d) Trinidad Head (2002). Panel (e) compares the daily aerosol concentrations at two sites over the Indian sea (2006): MCO_H and MCO_G. The ABC data in the panels (a)–(d) are downloaded from ftp.cmdl.noaa.gov/aerosol/, and reference for the panel (e) is Ramanathan et al. (2007).

Table 2. Size distribution parameters for aerosols

Aerosol component	N_i	r_i (μm)	σ_i
Sulphate ($r < 0.05$ μm)[a]		0.025	1.4
Sulphate (r: 0.05–0.63 μm)[a]		0.079	1.4
Sea salt ($r < 0.05$ μm)[a]		0.015	1.4
Sea salt (r: 0.05–0.63 μm)[a]		0.054	1.4
Dust[b]	0.8542	0.05	1.65
	0.1457	0.27	1.67
	7.3e-5	4.0	2.40
Fossil fuel OM/BC[c]	0.4286	0.005	1.5
	0.5714	0.08	1.7
	1.e-6	2.5	1.65
Biomass OM/BC and natural OM[d]	0.9987	0.0774	1.402
	1.3e-3	0.336	1.383
	2.8e-4	0.9577	1.425

[a]Bates et al. (2002), [b]d'Almeida et al. (1991), [c]Radke et al. (1988) and [d]Anderson et al. (1996).

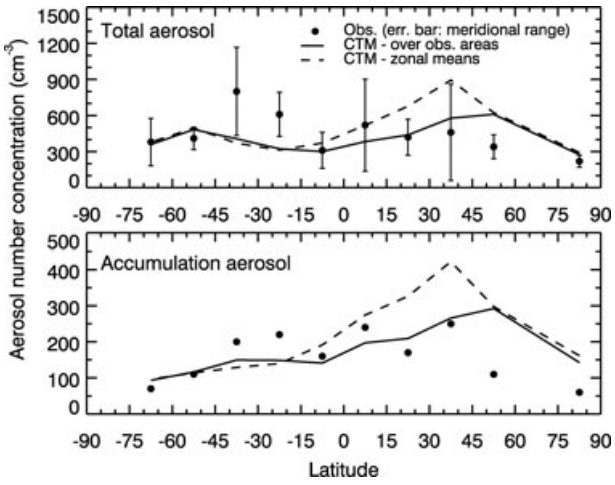

Fig. 4. The latitude distribution of the CTM-simulated aerosol number concentrations (solid lines) compared with a 30-yr observational marine aerosol data (dots) over the remote oceans (Heintzenberg et al., 2000), for total (top panel) and accumulation-mode (bottom panel) aerosols. Also shown are the simulated zonal means over the oceans (dashed line).

Indian Ocean and the Pacific Ocean (Ramanathan et al., 2007). Aerosol number concentrations are calculated from the predicted aerosol mass concentrations, using the observed climatological size distributions for each aerosol type listed in Table 2 (Radke et al., 1988; d'Almeida, 1991; Anderson et al., 1996; Bates et al., 2002). The individual size distribution is constant, but the size spectrum of total aerosol number concentrations varies in space and time with the changing fractional contributions by each aerosol component. In Fig. 3a, the distinctive annual cycle observed at Maldives (MCO_H) is captured by the CTM, for example, the total aerosol number concentration decreases from the very high concentrations (>1500 cm^{-3}) during the dry polluted winter monsoon season to much lower concentrations (<500 cm^{-3}) during the wet pristine summer monsoon season. The correlation coefficient between the simulations and the observations is 0.62 at this site. Large-scale spatial variations in aerosol concentrations are also simulated, transitioning from a frequently polluted site (Gosan) with year-round particle concentrations over thousands per cm^3 to the relatively remote sites (Mauna Loa and Trinidad Head) with several hundred particles per cm^3. The geometric (arithmetic) mean percent errors of the simulated daily mean aerosol number concentration relative to the observations are 57%, 83% and 70% at Maldives, Mauna Loa and Trinidad Head, respectively. The errors in the annual means are much smaller, about 35%, 19% and 2% at the above three cites. From March to June of 2006, aerosol surface measurements were made at two observatories located over the North and the S. Indian Ocean, MCO_H (6.78°N, 73.18°E) and MCO_G (0.69°S, 73.15°E) (Ramanathan et al., 2007). As shown in the Fig. 3e, the large north–south gradient in the observed aerosol concentrations between the two locations is also similarly depicted in the model predictions. The correlation coefficient between the model and surface measurements is 0.57 at MCO-H and 0.67 at MCO_G.

The latitudinal distributions of the simulated annual mean aerosol (total and accumulation-mode) number concentrations are compared in Fig. 4 with a comprehensive marine aerosol data set. This data set available at 15° × 15° grid cells is compiled from about 30-yr measurements over the remote oceans (Heintzenberg et al., 2000). Focusing first on observations, total aerosol concentration peaks around 45°S–30°S in the southern hemisphere (SH), whereas the accumulation-mode aerosols are nearly symmetric between the two hemispheres. The lower bias in the SH (15°–45°S) CTM simulations might be due to the neglect of biogenic emissions of marine organic aerosols. Other observational studies suggest this to be an important marine aerosol source during biologically active periods at Mace Head (O'Dowd et al., 2004). However, since the observations over the remote oceans are from ship measurements, there are likely to be sampling biases in representing annual means. The simulated total and accumulation-mode aerosol concentrations between 45° and 60°N are larger than the observations, probably because the observational data excluded measurements for polluted air masses at coastal stations in these latitudes. Overall, the simulated aerosol concentrations are shown within the meridional range of the observations for 7 out of the 12 latitude bands. Another point to note is that the observations do not represent the true zonal means over the ocean. The potential observational bias can be inferred by comparing the solid line (simulated values over the observational regions) with the dashed line (the true zonal mean of the model simulations). The anthropogenic

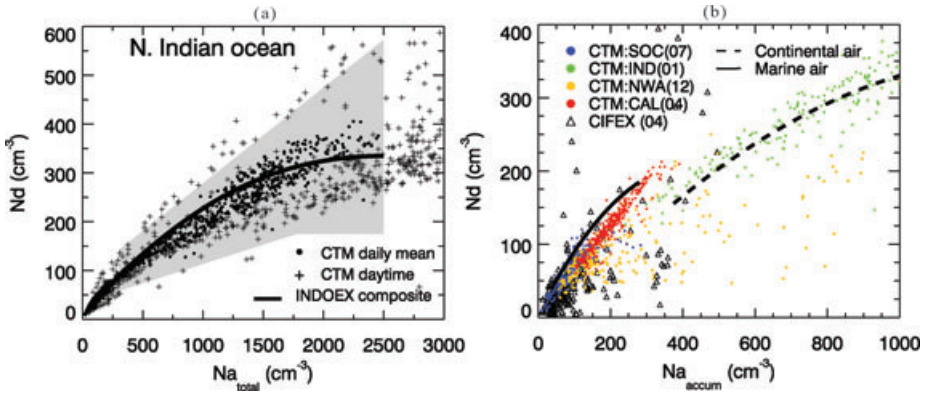

Fig. 5. The increase of cloud droplet number concentration (N_d) with (a) total (N_{atotal}) and (b) accumulation-mode (N_{aaccum}) aerosol number concentration. In (a), the INDOEX composite scheme is represented by the solid line, while the grey-shaded area denotes the range of the in situ aircraft data. The simulated daily mean and daytime values are indicated by dot and plus symbols, respectively. Panel (b) shows the CIFEX aircraft measurements (open triangles) and the empirical relationships derived from various aircraft measurements for marine (dashed line) and continental (solid line) air masses over the oceans. Also shown are daytime simulations over the S. Ocean (SOC), N. Indian Oceans (IND), NW Atlantic (NWA) and N. Californian coast (CAL). Number in the parentheses indicates the month displayed, that is, 01 for January.

contribution is more evident in the calculated zonal mean aerosol number concentrations.

The cloud microphysics simulated by the CTM is examined next. Figure 5a depicts the increase in CDNC as a function of the simulated total aerosol number concentration over the N. Indian Ocean (67.5°–75°E, 6°S–12°N). The model simulations include daily means and daytime values. Also shown are in situ aircraft measurements from the INDOEX campaign during late February to early April in 1999. Trade cumuli are the most common clouds during the INDOEX, when aerosol size and composition change from the aged and polluted continental types to the clean marine aerosols along with the shift in the prevailing wind direction. It presents a good test case to evaluate the model cloud microphysics under different atmospheric conditions. Figure 5a shows that the calculated daily mean CDNC agree within 15% compared with the derived empirical composite scheme (Ramanathan et al., 2001). The daytime aerosol and cloud concentrations predicted by the global model also largely fall into the uncertainty range of the in situ aircraft data, marked by the grey-shaded area (Heymsfield and McFarquhar, 2001).

Figure 5b compares the calculated daily mean CDNC with accumulation-mode aerosol concentrations for four typical marine stratus/stratocumulus regions and months (Klein and Hartmann, 1993): S. Ocean (46°–60°S, 0°–30°W) in July, N. Indian Ocean (2°S–12°N, 67.5°–75°E) in January, NW Atlantic (36°–46°N, 45°–60°W) in December, and the N. Californian coast (36°–44°N, 122.5°–130°W) in April. Also shown are *in situ* aircraft measurements from the CIFEX campaign (Wilcox et al., 2006) and the empirical relationships derived from multiple aircraft measurements over the Atlantic (Martin et al., 1994). Consistent with the observed relationships representative of both polluted continental and clean marine air masses, the CTM simulations indicate more rapid increases in CDNC with increasing aerosol number concentration for relatively clean marine clouds over the S. Ocean and off the California coast, as opposed to the more polluted regions, that is, the N. Indian Ocean and the NW Atlantic. Furthermore, the CIFEX aircraft data indicates approximately 50% of the accumulation-mode aerosol particles activated to form cloud droplets off the coast of California, and the similar activation ratio is simulated by the CTM. This shows that the CTM is capable of largely reproducing the observed regional variability in cloud microphysical properties in marine stratus, arising from differences in regional aerosol chemistry and microphysics. On the other hand, a significant fraction of the predicted aerosol and CDNC off the N. California coast are above the range of the CIFEX observations, although their relationships seem to follow a similar slope. It could be because the CTM uses a climatological size distribution to distribute the sulphate mass generated in the gas-phase chemistry. While it is a good representation for the aged aerosol layer or cloud-processed aerosols, it overestimates the accumulation-mode concentration (thus droplet activation) for freshly formed (6–24 h) particles, that is, North America continental aerosols whose median radius size is only about 30 nm (Roberts et al., 2006). This error should become smaller for remote marine environment away from the aerosol sources. Nevertheless, the calculated column-mean cloud droplet effective radius ($\frac{3\times CLWP}{2\rho_w \tau} = 10.2\ \mu$m) is only moderately lower than the mean value of 11.1 μm derived from the CIFEX aircraft measurements.

Comparisons of the simulated aerosol number concentrations as well as the simulated aerosol–droplet relationships with various ground-based and aircraft data have not revealed major flaws in the simulations, and indeed the simulations mostly agree with the field data within experimental errors. This sets the stage for

comparing the regional scale variations in the simulated cloud optical properties next.

4. Cloud optical properties of marine warm clouds

The SSM/I microwave measurements of CLWP represent the column-integrated water path for liquid phase clouds, which are to be found at altitudes with pressure, $P > 500$ hPa (except for deep convective clouds). However, these microwave data may also include mixed-phase clouds, which contain both liquid water and melting ice. The CTM has a microphysics treatment for liquid phase clouds, but does not have a separate treatment for mixed phase clouds. Thus the mixed phase clouds in the CTM would be counted as liquid phase clouds. In order to account for this parametrization problem, both the liquid phase and the mixed phase CODs from MODIS are combined (weight-averaged by their corresponding cloud fractions), when we compare CTM simulations with MODIS observations. For low-level cloud systems located at $P > 700$ hPA, such as the marine stratus, the stratocumulus and shallow trade-Cus, have only liquid phase clouds, and the comparison between CTM and MODIS is more rigorous. Hence, we examine these low-level clouds separately in Section 5. The conclusions we infer about the CTM treatment of aerosol–cloud interactions are made only when they are substantiated by the analyses at all three scales: hemispherical means; geographical patterns and localized analyses of the low-level cloud systems. Here after in the paper, the CTM simulations, MODIS and SSM/I satellite observations will be denoted by CTM, Obs_M and Obs_S, respectively.

4.1. Global and hemispherical means

Table 3 compares the global and hemispherical means of fine-mode AOD at 550 nm and CODs with available satellite observations over the oceans. To avoid the uncertainties in satellite retrieved values for polar regions, the comparison is restricted only to the averages over the 45°N–45°S latitude band. The models results, however, are shown for this limited band as well as for the global (pole to pole) means. The simulated AODs agree within 10% with the MODIS values (Obs_M). Moreover, the AODs over the NH oceans are larger than the SH ocean values by about 50% for both MODIS and CTM. The CTM suggests that this north to south asymmetry is due to the much larger role of anthropogenic aerosols in the NH (compare the CTM values for all aerosols with that for just the natural aerosols for

Table 3. Annual mean fine-mode aerosol optical depth at 550 *nm* and cloud optical properties from the chemical transport model simulations (CTM) and satellite observations (Obs_M for MODIS and Obs_S for SSM/I) over the oceans

	All latitudes		Between 45°S and 45°N	
	CTM–all aerosols	CTM–natural aerosols only	CTM–all aerosols	Obs_M or Obs_S
Fine-mode aerosol optical depth (550 nm)				
NH oceans	0.094	0.044	0.091	0.094
SH oceans	0.061	0.047	0.055	0.061
Global oceans	0.075	0.046	0.071	0.076
Cloud droplet number concentration (cm^{-3})				
NH oceans	167	96	169	
SH oceans	111	103	100	
Global oceans	133	100	131	
Cloud liquid water path ($g\ m^{-2}$)				
NH oceans	97	97	101	102(152)[a]
SH oceans	95	95	103	105(141)
Total oceans	96	96	102	104(146)
Column-mean droplet effective radius (μm)				
NH oceans	9.7	12.4	10.4	12.1[b]
SH oceans	11.2	11.9	12.9	13.0
Total oceans	10.7	12.1	11.8	12.7
Cloud optical depth				
NH oceans	15.2	11.8	14.7	12.6
SH oceans	12.9	12.3	12.1	12.1
Total oceans	13.8	12.1	13.2	12.3

[a]SSM/I microwave data are shown, and the numbers in parentheses denote the CLWP calculated from the MODIS-retrieved optical depth and effective radius by $\frac{2}{3}\rho_w \tau R_{eff}$.

[b]The column-mean droplet effective radius is estimated from the SSM/I CLWP and the MODIS COD by $\frac{3\times CLWP}{2\rho_w \tau}$.

global means). In fact, for just the natural aerosols, the SH value is slightly larger by about 7% (0.047 for SH versus 0.044 for NH). Anthropogenic aerosols increase the SH AOD by 0.014 (=0.061–0.047) compared with its impact on NH, where it increases AOD by 0.05 (=0.094–0.044). The simulation of the hemispherical mean AODs as well as the interhemispheric asymmetry builds confidence in the CTM's ability to simulate aerosol optical properties globally.

Cloud properties are examined next. There are no global observations for CDNC. The simulated CDNC for the NH is larger than the SH value by about 50%, similar to the simulated AOD trend. For example, for the 45°N–5°S band, the NH CDNC is 169 cm^{-3}, whereas the SH CDNC is only 100 cm^{-3}. According to the CTM, the larger NH value is entirely due to the larger amount of anthropogenic aerosols in the NH. The interhemispheric asymmetry in CLWP is less than 3% and is within experimental errors. Since the CTM column-integrated CLWP is constrained by satellite observations (SSM/I), the global and hemispheric mean CTM values are in close agreement with the satellite derived values. The simulated effective cloud droplet radius and COD are in surprisingly close agreement with the observed values for the SH, but differ systematically by about 15% for the NH. The effective droplet radius is smaller, and the COD is correspondingly larger. As a result, while the model simulates the interhemispheric differences in the effective radius (smaller in the NH) and COD (larger in the NH), it exaggerates these differences significantly. In the model, the interhemispheric differences arise solely from anthropogenic aerosols, which raises the possibility that the CTM (and possibly other global models) treatment of aerosol effects on COD (and thus albedo) suffers from a substantial positive bias. Such an inference has also been made by an earlier study (Quaas et al., 2008). Given the fact that the observed as well as the CTM simulated differences are comparable to the experimental errors in satellite derived values (about 10% or larger), we would resist the temptation to explore this issue further. However, similar systematic biases show up in the regional comparisons as described next. Except for the discrepancy in the simulated interhemispheric asymmetries in CODs and effective radius, the simulation of AODs and CODs lend credence to the performance of the CTM treatment of aerosol chemical and optical properties, as well as the treatment of aerosol effects on cloud microphysical and optical properties.

4.2. *Geographical patterns*

In Fig. 6, the simulated COD for marine warm clouds depicts broadly similar geographical patterns to the Obs_M retrievals. Clouds over the extra-tropical and tropical oceans appear to be optically thick with the COD larger than 12.5, while subtropical marine stratus and stratocumulus clouds generally have lower or intermediate optical depth between 5 and 12.5. Maximum optical depth is associated with the deep convective clouds over the tropical oceans, exceeding 12.5 in both the CTM simulations and the satellite data. Figure 7 compares the spatial distribution of the annual mean fine-mode AODs, and together they demonstrate the extent to which spatial distribution of CODs is correlated with spatial variations in aerosols. The CTM predicts significant optical depths for clouds over the northern Pacific and Atlantic Oceans, collocating with the presence of highly concentrated anthropogenic aerosols (AOD > 0.05) downwind of the major continental pollution sources in East Asia and North America. Such anthropogenic influences are also indicative in the Obs_M especially over the northwestern Pacific. In the SH oceans between 40°S and 60°S, both the simulated and the retrieved CODs suggest the existence of an extensive band of warm clouds, which are also optically thick (COD > 12.5). The large SH CODs seemingly correspond to the large production of sea salt and DMS-generated natural sulphate aerosols in these latitudes owing to the strong prevailing SH westerlies. The simulated and observed regional fine-mode AODs are visibly larger than the background AODs (<0.02). The enhancement in the NH AODs due to anthropogenic influences simulated by the

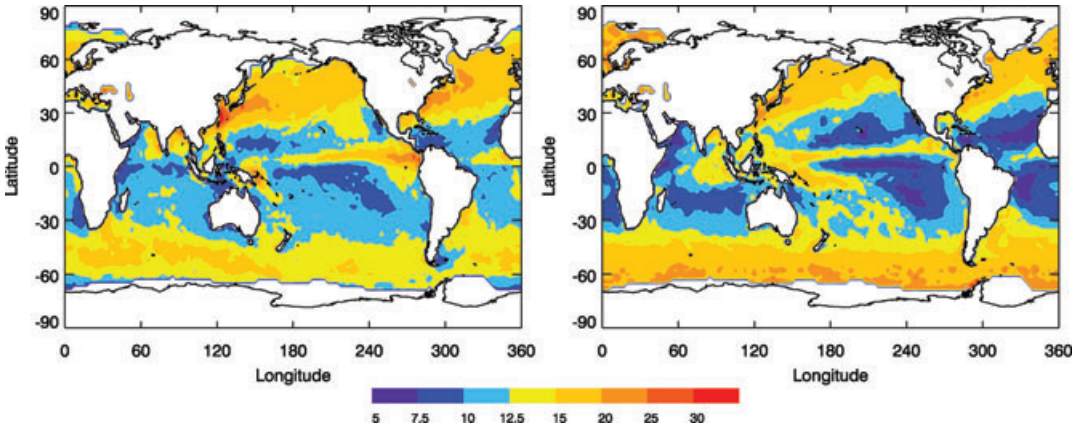

Fig. 6. Left-hand panel: the CTM-simulated annual mean cloud optical depth for marine warm clouds with top lower than 500 hPa. Right-hand panel: the MODIS annual mean cloud optical depth averaged for both liquid- and mixed-phase clouds over the oceans.

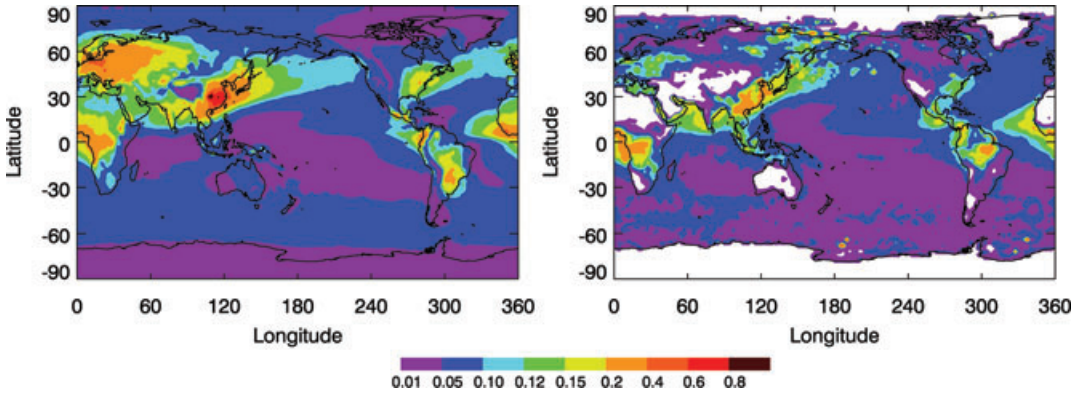

Fig. 7. Annual mean fine-mode aerosol optical depth at 550 nm. Left-hand panel: the CTM simulations; Right-hand panel: MODIS. White colour in the MODIS data indicates areas without quality retrievals.

CTM is similarly revealed in the observations, as well as the relatively lower AODs over the N. Atlantic Ocean relative to the N. Pacific Ocean. The spatial variations of COD corresponding to the enhanced anthropogenic AODs however, appear to be less pronounced in the Obs_M compared with the CTM calculations.

The geographic distributions and hemispheric means of COD and fine-mode AOD demonstrate correlated variations in both CTM simulations and satellite observations. Such correlations on hemispherical and regional scales enable us to isolate the effect of variations in aerosol sources on the observed regional and hemispheric differences in cloud optical properties, particularly since we have prescribed the CLWP.

5. Aerosol–cloud interactions in subtropical marine stratus clouds

Subtropical marine stratus clouds, usually single-layer clouds capped out at 700 hPa with extensive coverage, are least affected by the model assumptions on thermophase or overlapping of clouds. Optical retrievals based on the radiance measurements (Obs_M) are also best quantified for these clouds. Therefore, comparison of the model simulations with satellite observations over the subtropical marine stratus regions is a more informative and perhaps a more reliable indicator of the simulated aerosol–cloud interactions. The regional analyses starts off with an examination of the daily variability and focuses on two strato-cumulus regions: off the western coasts of S. America (SAM: 20°S–6°S, 70°W–85°W) in September, and California (CAL: 24°N–36°N, 120°W–135°W) in April. We then analyse the seasonal variations of COD, for which we also include a trade-cumulus region in the N. Indian Ocean (IND: 2°S–12°N, 67.5°E–75°E).

5.1. Simulation of daily variability

The frequency distributions of daily daytime CLWP from the CTM simulations and two satellite observations are shown together in Fig. 8. The MODIS CODs are 1° daily data (MOD08-D3) for single-layer liquid water clouds, and they are aggregated to the large model grids, weighted by the single-layer liquid cloud fractions. CLWP is calculated from the MODIS COD (τ) and cloud-top CDR (r_e) data from the expression $\frac{5\rho_w}{9}\tau \times r_e$. This formula assumes adiabatic stratification in non-drizzling marine stratus clouds, and the obtained CLWP is shown to generally agree better with the AMSR-E (a successor to the SSM/I) microwave measurements than the MODIS level-3 data by Bennartz (2007). The rationale for including CLWP from MODIS is as follows: the SSM/I data is a column-integrated product for all liquid phase clouds, and more importantly, it cannot distinguish liquid water content in drizzle drops from cloud droplets, while only the latter has a main impact on the COD simulations. MODIS CLWP, while it may not be an accurate estimate of the actual CLWP due to the assumption made for the liquid water content profiles, should capture the daily and seasonal variability of single layer clouds. In short, reality for a single layer cloud should lie somewhere in between MODIS and SSM/I CLWPs.

CLWP is highly variable in both satellite data sets with standard deviations (*SD*) nearly 40% of each of their mean values, and the CTM captures this variability in the daily CLWP distributions. The fine-mode AOD (middle panels) reveals an important pattern. The model correctly simulates that the peak fine-mode frequency occurs at about 0.1 for CAL and about 0.05 for SAM. However, the observed distribution has a fatter tail at higher AOD values than the simulated AODs. The underestimated frequencies at large fine AOD values (>0.12) may be the main reason for the low-biased mean AOD predictions compared with the Obs_M (Table 3), but it should not impact the COD estimates significantly since the aerosol effects on COD are mostly susceptible to the low AOD conditions.

The simulated COD daily distribution is very similar for the SAM region, except for a slight shift towards the right-hand side (large values). This shift is worsening in the simulations for the CAL region. The standard deviation of the simulated distribution is within 10% to observations for the SAM region,

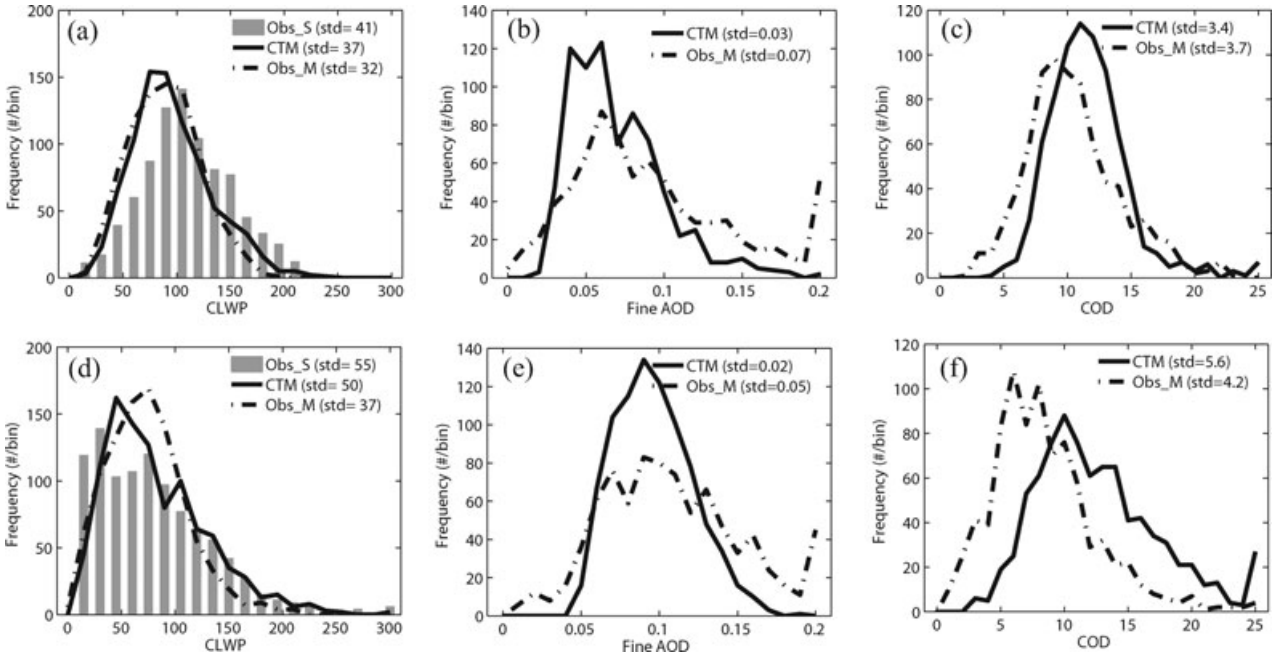

Fig. 8. Frequency distribution of the daytime CLWP, fine-mode AOD, and COD from the satellite observations (Obs_M and Obs_S) and the CTM simulations, over the marine stratus regions: (a)–(c) SAM in September, and (d)–(f) CAL in April.

while it is larger by about 30% for the CAL region. As a result, the estimated monthly mean COD over the SAM region agree reasonably well with the Obs_M satellite retrievals, with a geometric mean percent error of 6% and a RMS error of 1.6. Given the 10–20% uncertainty usually in these satellite-retrieved COD, the aerosol–cloud interactions, including from aerosols to droplet activation to drizzle formation, are simulated over this area. The comparison of COD over the CAL region however indicates an average overestimation of 42%. The geometric mean error is larger than the maximum uncertainty estimated to be potentially associated with CLWP used (there is about 26% difference between the Obs_S and Obs_M data). The overestimation is consistent with the cloud microphysics comparison off the N. Californian coast (discussed in the Section 3), so it may be likely explained by the aerosol size distributions assumed in the droplet activation. Since most of the current CTMs or global climate models follow an approach similar to that adopted here, their estimated aerosol cloud albedo effects could be possibly subject to a similar overestimation, even with the properly represented cloud dynamics.

Another likely reason for the shift to the right-hand side in the COT distribution is due to the deficiency in the drizzle parametrization. Without in situ measurements in place to evaluate the drizzle parametrization, we resort to sensitivity studies on the critical droplet size (dr_{crit}), which is used to determine the on-set of drizzle formation. Figure 9 illustrates the drizzle effect on the frequency distribution of CODs in the region CAL (April), by comparing three CTM simulations: the standard run (dr_{crit} = 7.5 μm), without drizzle formation (dr_{crit} = infinity)

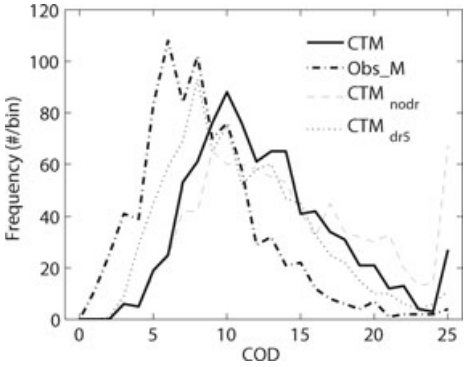

Fig. 9. Drizzle effect in the CAL region (April): frequency distribution of the daytime COD from the Obs_M (thick dash–dotted line) and the CTM simulations (standard run: thick solid line; without drizzle formation: dashed line; drizzle critical droplet size (dr) of 5 μm: dotted line).

and dr_{crit} = 5 μm, with the satellite observations (Obs_M). Inclusion of the drizzle formation improves the model comparison with the satellite data by about 20–30%, because it reduces the calculated COD for clouds with significant CLWP (on the long tail of the CLWP distribution) by assigning some portion of the liquid water content to drizzle drops that scatter solar radiation much less efficiently. For the region CAL (or SAM), the overestimation in COD decreases from 63% (or 32%) with no drizzle formation to 41% (or 6%) with the implemented parametrization. Using a even smaller critical droplet size (5 μm), which is only half of that ($\sim$10 μm) suggested by aircraft experiments, the calculated regional mean COD in CAL is about +24% higher

than the Obs_M retrievals, which have uncertainties of 10–20%. Sensitivity studies clearly demonstrate that the uncertainty associated with the drizzle parametrization could contribute to the discrepancies between the estimated and observed COD.

5.2. *Seasonal cycle*

In this section, we examine the aerosol influence on the seasonal variations of COD. Figure 10 shows the monthly mean CODs, CLWPs and fine-mode AODs from the CTM and satellite observations over the three regions: SAM, CAL and IND. Since the CTM values are constrained by the SSM/I data on the monthly mean basis, they are almost equal to each other for total liquid water path over CAL and IND ('all clouds' in Figs. 10d and g); for SAM, there are about 9% discrepancies between SSM/I and CTM CLWPs, resulting from the time interpolation (Fig. 10a). For single-layer (1L) clouds in the subtropical regions such as SAM or CAL, differences between the constrained CTM CLWP and the Obs_M values inferred from the optical retrievals are mainly due to drizzle drops (excluding experimental errors); therefore, the simulation of COD is sensitive to the implemented drizzle parametrization. As shown in Figs. 10c and f, sensitivity runs with a smaller critical droplet size seem to help to reduce the differences between the simulated and Obs_M CODs in several months, when the COD estimates fall within the uncertainty ranges of the observations. Over the IND region, cloud types are not constant throughout the year, from scattered shallow trade cumuli to mesoscale deep convective cloud systems. Although the total CLWP in liquid phase clouds are constrained (Fig. 10g), uncertainty associated

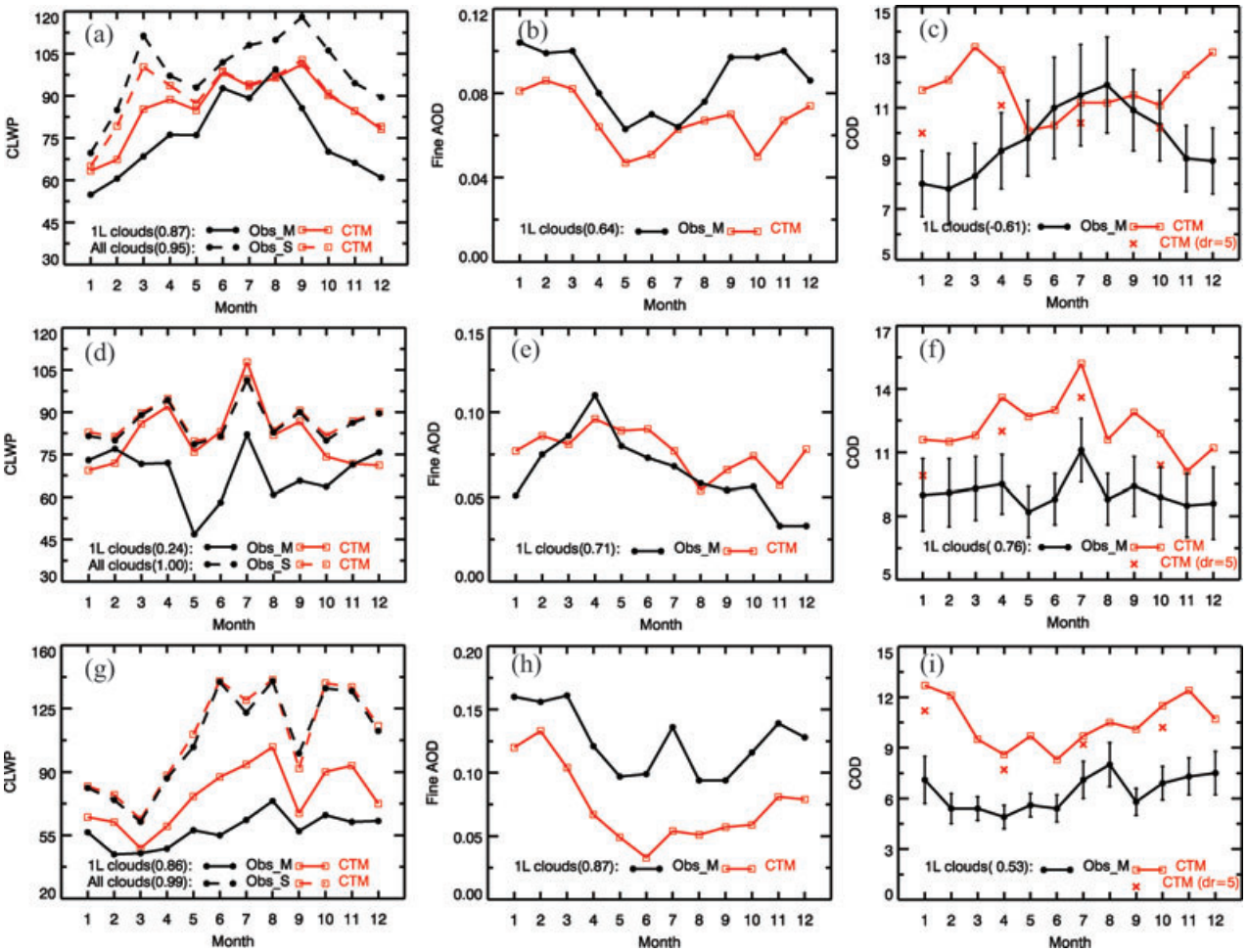

Fig. 10. Seasonal variations in the monthly mean CLWP, fine AOD, and COD over the regions of (a)–(c) SAM, (d)–(f) CAL and (g)–(i) IND. The CTM results (red solid line) and the Obs_M data (black solid line) are shown for aerosol and single-layer (1L) cloud properties. In the panels (a), (d) and (g), the Obs_S CLWP data (black dashed line) are also shown with the CTM total CLWP (red dashed line) for all the liquid phase clouds. Numbers in the parentheses are correlation coefficients between the simulated and observed values. Error bars in the panels (c), (f) and (i) indicate uncertainties in the Obs_M, and cross symbols represent the CTM simulations with critical droplet size (dr) of 5 μm for January, April, July and October.

with the parametrized cloud overlapping scheme or the 'known' low-bias in the MODIS-retrieved CODs are among the main contributors to the differences between CTM and the Obs_M CLWP for single-layer clouds.

Despite the differences in absolute values discussed, most importantly, Fig. 10 shows the seasonal cycles of CLWP and AOD simulated by the CTM correlate strongly with the satellite observations. For example, the calculated correlation coefficients for AOD are 0.64, 0.71 and 0.87 between the simulations and Obs_M retrievals for the regions of SAM, CAL and IND, respectively. For CLWP, the correlation coefficients between the CTM values and either Obs_S or Obs_M data are larger than 0.86, except for the single-layer clouds in CAL only, where the two satellite data sets do not correlate well. This shows that the constrained CTM generally captures the month-by-month variability in aerosol loadings and large-scale dynamic conditions thus enable us to examine their individual roles in determining the annual cycle of COD.

In the MODIS satellite observations, COD, not surprisingly, is predominately influenced by variations in CLWP, as the correlation coefficients (corr) between COD versus CLWP are larger than those between COD versus AOD for all three regions. Similarly, the CTM simulations also indicate stronger correlations to CLWP in CAL and IND. For example, in CAL, the corr of COD and CLWP is 0.64 (Obs_M) and 0.86 (CTM), larger than the corrs of 0.28 (Obs_M) and 0.44 (CTM) between COD and AOD. However, for SAM, the simulated CODs respond much more closely to the AOD changes than suggested by the observations. In addition to the uncertainty in the drizzle parametrization, the overly sensitivity of the simulated COD to increasing AOD from October to March (Figs. 10b and c) could be resulted from the neglect of biomass burning aerosols in the model cloud microphysics as it overlaps with the local burning season. Another possibility is that the long-range transported biomass burning aerosols by the high-level tropical easterlies does not interact with the marine boundary layer clouds until further to the west of the SAM region, but their presence above the clouds may affect the satellite retrieval of COD.

Although the aerosol influences on COD seem to be dominated by CLWP variations on the yearly cycle, it could be more important on a shorter time scale. Over IND, the increasing AOD from September to January due to the anthropogenic pollution plumes transported from the continental sources correlates with the enhancement in COD, with a corr of 0.73 in both CTM and Obs_M data. Meanwhile, the correlation between COD versus CLWP is less for 0.6 (Obs_M) and 0.21 (CTM), implying weaker influences from dynamic processes than aerosols. From February to April when the regional aerosol loadings declines as the prevailing wind direction switches, the correspondent reduction in COD is also observed more sensitive to the decreased AOD (corr = 0.99) than the increasing CLWP (corr = 0.81). The similar correlations are simulated by the CTM. Overall, in the above three regions, the month-by-month relative variability (defined as the ratio of the *SD* to its mean) of AOD is comparable (such as in SAM) or more significant (such as in CAL and IND) compared with that of CLWP, however, perturbations in CLWP (implicitly including aerosol indirect effect on cloud lifetime) are generally driving the corresponding changes in COD.

6. Summary

Cloud-radiative interactions are one of the largest sources of uncertainty in global climate change simulations. As a major contributor to the net cloud radiative forcing, optical properties of marine warm clouds are of great importance. Although early investigations have established the connection between aerosols and cloud radiative effects, they are far from being accurately quantified. One of the major difficulties has been identified as the model inability to account for the liquid water content in cloud. In this study, a cloud microphysics scheme is developed to simulate aerosol indirect effect in marine liquid water clouds with a global CTM. The simulated aerosol and CDNC are evaluated against various surface and aircraft measurements in the polluted and pristine marine environment. Using the CLWP constrained by the satellite-based SSM/I microwave measurements, the obtained COD is compared with the MODIS cloud retrievals to investigate aerosol and cloud interactions (mainly cloud albedo effect) in marine warm clouds at both global and regional scales.

The geographical distribution of the fine-mode AODs at 550 nm simulated by the CTM is shown to be generally consistent with the MODIS satellite observations. Their hemispherical annual means agree within 10% in both hemispheres. As a result, the simulated global mean COD for marine warm clouds (13.2) is 7% larger than the MODIS-retrieved value (12.3) over the oceans between 45°S and 45°N. Both the model simulations and the satellite observations similarly depict correlated variations in the spatial distribution of aerosol loadings and marine warm COD. The CTM also simulates large interhemispheric asymmetries: the NH aerosol number concentration is larger than the SH mean by ∼100%, fine-mode AOD (at 550 nm) is larger by 54%, cloud droplet number concentration is larger by 51%; COD is larger by 18% for marine warm clouds, while column-mean droplet effective radius is smaller by 13%. Meanwhile, the prescribed SSM/I CLWP used in the model simulations do not indicate such hemispheric differences. In the model, these differences are essentially driven by corresponding interhemispheric asymmetries in anthropogenic emission sources, because in the presence of just the naturally produced aerosols (sea salt and DMS-generated sulphate), optical depth of marine warm clouds simulated by the global model is slightly higher in the SH, with the consistent aerosol geographic distributions. The simulated hemispheric differences in cloud properties are consistently but less significantly revealed in the MODIS COD (+4%) and the CDR (−7%) inferred from MODIS COD and SSM/I CLWP.

Regional analyses are performed over the subtropical marine stratus regions (off the west coast of California and S.

America), where satellite cloud observations are best retrieved. These analyses provide insights into the CTM simulations of aerosols and influences on cloud properties. It shows that the uncertainties in the CTM-estimated COD are mainly associated with the monthly mean liquid water paths and the microphysical link between aerosols and clouds associated with aerosol size distribution. The simulated fine-mode AODs and the GCM-generated CLWP daily variabilities are reasonably represented by the CTM, compared with the satellite observations. The implemented drizzle parametrization improves the CTM estimates of COD by 20–30%, but not entirely. Moreover, the constrained CTM generally captures the seasonal variations in AOD and CLWP over the marine stratus/stratocumulus or trade cumuli regions, and indicates that the annual cycle of COD is driven mostly by variations in CLWP. The aerosol influence on COD changes is also implied by a stronger correlation than CLWP, during the winter monsoon over the N. Indian Ocean.

It is recognized that the model-estimated aerosol indirect effects on cloud albedo are usually more significant than that inversely derived from the space-based radiation measurements, as discussed in the recent IPCC report and recent studies (Quaas et al., 2008). We showed that with the CLWP constrained by the satellite microwave measurements, a global CTM, which is shown to perform well in modelling aerosol optical properties and their global distribution, could still overestimate cloud optical properties. Some of the model inefficiencies identified in this study regarding drizzle formation and aerosol size distributions are considered commonly existing in global aerosol or climate models. Improvements in modelling aerosol properties in cloud droplet formation at a global scale are anticipated to reduce the gap between model estimates of aerosol indirect effect and the satellite observations. On the other hand, the general consistency between the simulated and observed hemispheric differences and seasonal variations in marine warm cloud optical properties support the simulated aerosol effects on clouds.

A similar approach can be applied to examine aerosol–cloud interactions in mixed phase and ice clouds. The aerosol–cloud microphysics scheme should also be extended to include other aerosol types such as dust coated with soluble material, aged carbonaceous aerosols, etc. Finally, improvements in cloud dynamics such as entrainment-mixing processes, as suggested by field observations, are also necessary. More importantly, improved satellite measurements of cloud characteristics at the macro- and microscale (e.g. CloudSat data; Stephens et al., 2008) should be incorporated with the global modelling study of aerosol–cloud interactions as they become available.

7. Acknowledgments

This research was supported by NSF Atmospheric Sciences Program under the grant ATM-0721142. The Atmospheric Brown Cloud (ABC) observatories were funded by NOAA. MODIS and CERES data sets were provided by the NASA Goddard and Langley DAAC, respectively. SSM/I data were produced by Remote Sensing Systems.

8. Appendix

A.1. Global chemical transport model

The CTM uses a flux-form semi-Lagrangian advection scheme (Lin and Rood, 1996). Dry deposition of aerosol particles uses a resistance-in-series parametrization following Zhang et al. (2001). The wet deposition scavenging parametrization is based on the Harvard wet scavenging model (Mari et al., 2000; Liu et al., 2001). In convective updrafts, the fraction of tracer scavenged is calculated based on the rate constant for conversion of cloud condensate (including liquid and ice) to precipitation (assumed to be 0.005 s^{-1}) and the fraction of tracer present in the cloud condensate f_i (scavenging efficiency), that is, the scavenging efficiencies of sulphate, nitrate, ammonium, and carbonaceous aerosol are 1.0, 1.0, 1.0 and 0.4, respectively. In addition, the fraction of a tracer lost due to rainout (in-cloud scavenging) depends on the wet scavenging efficiency of the tracer, the horizontal area-fraction of the grid box experiencing precipitation, and conversion rate of cloud condensate to precipitation. Washout (below-cloud scavenging) by large-scale precipitation is computed as a first-order loss process using a rate which is calculated by multiplying a constant scavenging efficiency, 0.1 mm^{-1}, by the precipitation rate (in mm h^{-1}) in the precipitating fraction of the grid box (Balkanski et al., 1993). Resuspension is calculated in any grid box where there is net evaporation of precipitation. A fraction (assumed to be half) or total of the tracer precipitating from above is released in the grid box to reflect the partial or total evaporation of precipitation, respectively.

There are large uncertainties associated with the existing characterizations of sea salt aerosol production from the breaking waves over the oceans (Lewis and Schwartz, 2004). For example, there are about a factor of 7 differences in the generated emission fluxes by emission schemes based on oceanic whitecaps, which are commonly adopted in numerical models for sea salt generation. Besides Monahan et al. (1986), the flux expression given by Clarke et al. (2006) is also examined, which is derived from surf-zone measurements mainly for fine and ultrafine sea salt particles. Between the two schemes, the combination of the Monahan et al.'s sea salt flux function and the ERA-40 10-m wind speed data tends to give better agreements between the modelled and observed sea salt mass concentrations in the submicron size range (Bates et al., 2002), which is mostly important for cloud droplet activation. Therefore, the expression by Monahan et al. (1986) is used and extrapolated to include the emissions of ultrafine aerosols.

A.2. Cloud microphysics

First, aerosol activation spectrum (represented by CCN as a function of supersaturation ratio, S) is computed from Köhler

theory, as a function of aerosol number concentrations (varying between 10 and 5000 cm^{-3}), and chemical composition in the two size ranges: Aitken (particle diameter, $D_p < 0.1\ \mu m$) and accumulation ($0.1\ \mu m < D_p < 1.25\ \mu m$). The internal mixtures of sulphate and sea salt aerosols from both natural and anthropogenic sources are assumed to activate in the droplet formation. Each of the calculated aerosol activation spectrum (CCN-S) is divided into multiple segments, so that every segment can be approximated by the power-law relationship, $CCN = CS^k = bN_aS^k$, in which N_a is the total aerosol number concentration of the sulphate and sea salt mixture. For such power-law relationships, Twomey (1959) derived analytic solutions for cloud droplet number concentration (N_d) and the maximum supersaturation (S_{max}) in ascending,

$$N_d(W) = C^{2/(k+2)} \left[\frac{6.9 \times 10^{-2} W^{3/2}}{kB\left(\frac{k}{2}, \frac{3}{2}\right)} \right]^{k/(k+2)} \quad \text{(A1)}$$

$$S_{max}(W) = C^{-1/(k+2)} \left[\frac{6.9 \times 10^{-2} W^{3/2}}{kB\left(\frac{k}{2}, \frac{3}{2}\right)} \right]^{1/(k+2)}, \quad \text{(A2)}$$

where B is the Beta function, and W is the in-cloud updraft velocity. Thus a smoothed empirical relationship linking N_d to W can be numerically obtained, corresponding to each specific aerosol activation spectrum. Finally, a lookup table of the grid-mean cloud droplet concentration ($\overline{N_d}$) is generated for various aerosol activation spectrums,

$$\left\{ \begin{array}{c} \overline{N_d} = \sum_i N_d(W_i) \times f(\omega_i) \\ W_i = \omega_{ls} + \omega_i \end{array} \right\}, \quad \text{(A3)}$$

where ω_{ls} denotes the large-scale mean vertical velocity in a grid box. $f(\omega_i)$ denotes the subgrid variability of the in-cloud updraft velocity (ω_i), and is represented by a probability density function (PDF) with a mean velocity of 0.14 ms^{-1} and a standard deviation of 0.11 ms^{-1}. The updraft PDF parameters were the minimum values observed for marine stratocumulus during CSTRIPE (Meskhidze et al., 2005). For clouds with small cloud fractions (<5%), a more convective updraft velocity distribution is used following that observed in trade cumulus during INDOEX (McFarquhar and Heymsfield, 2001). At each time step, cloud droplet number concentration in a single grid box is interpolated from the look-up table, depending on the input parameters interactively calculated by the CTM, that is, CN concentration, ratio of sulphate aerosol to sea salt aerosol in the two size ranges, in-cloud updraft velocity and temperature.

References

Abdul-Razzak, H. and Ghan, S. J. 2000. A parameterization of aerosol activation. 2: multiple aerosol types. *J. Geophys. Res.* **105**(D5), 6837–6844, doi:10.1029/1999JD901161.

Abdul-Razzak, H. and Ghan, S. J. 2002. A parameterization of aerosol activation. 3: sectional representation. *J. Geophys. Res.* **107**(D3), 4026–4031, doi:10.1029/2001JD000483.

Abdul-Razzak, H., Ghan, S. J. and Rivera-Carpio, C. 1998. A parameterization of aerosol activation. 1: single aerosol type. *J. Geophys. Res.* **103**(D6), 6123–6132, doi:10.1029/97JD03735.

Ackerman, A. S., Kirkpatrick, M. P., Stevens, D. E. and Toon, O. B. 2004. The impact of humidity above stratiform clouds on indirect aerosol climate forcing. *Nature* **432**, 1014–1017.

Albrecht, B. A. 1989. Aerosols, cloud microphysics, and fractional cloudiness. *Science* **245**, 1227–1230.

Anderson, B. E., Grant, W. B., Gregory, G. L., Browell, E. V., Collins, J. E., Jr. and co-authors. 1996. Aerosols from biomass burning over the tropical South Atlantic region: distributions and impacts. *J. Geophys. Res.* **101**(D19), 24117–24138, doi:10.1029/96JD00717.

Andreae, M. O., Rosenfeld, D., Artaxo, P., Costa, A. A., Frank, G. P. and co-authors 2004. Smoking rain clouds over the Amazon. *Science* **303**, 1337–1342.

Andres, R. J. and Kasgnoc, A. D. 1998. A time-averaged inventory of subaerial volcanic sulfur emissions. *J. Geophys. Res.-Atmos.* **103**(D19), 25251–25261.

Balkanski, Y. J., Jacob, D. J., Gardner, G. M., Graustein, W. C. and Turekian, K. K. 1993. Transport and residence times of tropospheric aerosols inferred from a global three-dimensional simulation of 210Pb. *J. Geophys. Res.* **98**(D11), 20573–20586, doi:10.1029/93JD02456.

Bates, T. S., Coffman, D. J., Covert, D. S. and Quinn, P. K. 2002. Regional marine boundary layer aerosol size distributions in the Indian, Atlantic, and Pacific Oceans: a comparison of INDOEX measurements with ACE-1, ACE-2, and Aerosols99. *J. Geophys. Res.* **107**(D19), 8026–8040, doi:10.1029/2001JD001174.

Bennartz, R. 2007. Global assessment of marine boundary layer cloud droplet number concentration from satellite. *J. Geophys. Res.* **112**, D02201, doi:10.1029/2006JD007547.

Chameides, W. L., Luo, C., Saylor, R., Streets, D., Huang, Y. and co-authors. 2002. Correlation between model-calculated anthropogenic aerosols and satellite-derived cloud optical depths: Indication of indirect effect? *J. Geophys. Res.* **107**(D10), doi:10.1029/2001JD00208.

Chin, M., Ginoux, P., Kinne, S., Torres, O., Holben, B. N. and co-authors. 2002. Tropospheric aerosol optical depth from the GOCART model and comparisons with satellite and Sun photometer measurements. *J. Atmos. Sci.* **59**, 461–483.

Chuang, C. C. and Penner, J. E. 1995. Effects of anthropogenic sulfate on cloud drop nucleation and optical properties. *Tellus* **47B**, 566–577, doi:10.1034/j.1600-0889.47.issue5.4.x.

Clarke, A. D., Owens, S. R. and Zhou, J. 2006. An ultrafine sea-salt flux from breaking waves: implications for cloud condensation nuclei in the remote marine atmosphere. *J. Geophys. Res.* **111**, D06202, doi:10.1029/2005JD006565.

Coakley, J. A., Bernstein, R. L. and Durkee, P. A. 1987. Effect of ship-stack effluents on cloud reflectivity. *Science* **237**, 1020–1022.

Conover, J. H. 1966. Anomalous Cloud Lines. *J. Atmos. Sci.* **23**, 778–785.

d'Almeida, G. A., Koepke, P. and Shettle, E. P. 1991. *Atmospheric Aerosols: Global Climatology and Radiative Characteristics*, A. Deepak Pub., Hampton, VA.

Feng, Y. and Penner, J. E. 2007. Global modeling of nitrate and ammonium: interaction of aerosols and tropospheric chemistry. *J. Geophys. Res.* **112**, D01304, doi:10.1029/2005JD006404.

Feng, Y., Penner, J. E., Sillman, S. and Liu, X. 2004. Effects of cloud overlap in photochemical models. *J. Geophys. Res.* **109**, D04310, doi:10.1029/2003JD004040.

Forster, P., Ramaswamy, V., Artaxo, P., Berntsen, T., Betts, R. and co-authors. 2007. Changes in atmospheric constituents and in radiative forcing. In: *Climate Change 2007: The Physical Science Basis. Contribution of Working Group I to the Fourth Assessment Report of the Intergovernmental Panel on Climate Change* (eds S. Solomon and co-editors). Cambridge Univ. Press, Cambridge, UK and New York, NY, USA.

Gerber, H. E. 1985. Relative-humidity parameterization of the Navy Aerosol Model (NAM). In: *NRL Rep*. 8956, Natl. Res. Lab., Washington, DC.

Ghan, S. J., Chung, C. C. and Penner, J. E. 1993. A parameterization of cloud droplet nucleation. Part I: single aerosol type. *Atmos. Res.* **30**, 198–221.

Ghan, S. J., Chuang, C. C., Easter, R. C. and Penner, J. E. 1995. A parameterization of cloud droplet nucleation. 2: multiple aerosol types. *Atmos. Res.* **36**, 39–54.

Han, Q. Y., Rossow, W. B. and Lacis, A. A. 1994. Near-global survey of effective droplet radii in liquid water clouds using isccp data. *J. Clim.* **7**, 465–497.

Harrison, E. F., Minnis, P., Barkstrom, B. R., Ramanathan, V., Cess, R. D. and co-authors. 1990. Seasonal-variation of cloud radiative forcing derived from the earth radiation budget experiment. *J. Geophys. Res.-Atmos.* **95**(D11), 18687–18703.

Heintzenberg, J., Covert, D. C. and Van Dingenen, R. 2000. Size distribution and chemical composition of marine aerosols: a compilation and review. *Tellus* **52B**, 1104–1122.

Heymsfield, A. J. and McFarquhar, G. M. 2001. Microphysics of INDOEX clean and polluted trade cumulus clouds. *J. Geophys. Res.-Atmos.* **106**(D22), 28653–28673, doi:10.1029/2000JD900776.

Illingworth, A. J., Hogan, R. J., O'Connor, E. J., Bouniol, D., Brooks, M. E., Delanoe, J. and co-authors. 2007. CLOUDNET, Continuous evaluation of cloud profiles in seven operational models using ground-based observations. *Bull. Am. Meteorol. Soc.*, **88**, 883–898.

Jacobson, M. Z. 1999. Studying the effects of calcium and magnesium on size-distributed nitrate and ammonium with EQUISOLV II. *Atmos. Environ.* **33**, 3635–3649.

Kaufman, Y. J. and Nakajima, T. 1993. Effect of Amazon smoke on cloud microphysics and albedo–analysis from satellite imagery. *J. Appl. Meteorol.* **32**, 729–744.

Kettle, A. J. and Andreae, M. O. 2000. Flux of dimethylsulfide from the oceans: a comparison of updated data seas and flux models. *J. Geophys. Res.-Atmos.* **105**(D22), 26793–26808.

Kinne, S., Schulz, M., Textor, C., Guibert, S., Balkanski, Y. and co-authors. 2006. An AeroCom initial assessment–optical properties in aerosol component modules of global models. *Atmos. Chem. Phys.* **6**, 1815–1834.

Klein, S. A. and Hartmann, D. L. 1993. The Seasonal Cycle Of Low Stratiform Clouds. *J. Clim.* **6**, 1587–1606.

Lance, S., Nenes, A. and Rissman, T. A. 2004. Chemical and dynamical effects on cloud droplet number: implications for estimates of the aerosol indirect effect. *J. Geophys. Res.-Atmos.* **109**, D22208, doi:10.1029/2004JD004596.

Lewis, E. R. and Schwartz, S. E. 2004. *Sea Salt Aerosol Production: Mechanisms, Methods, Measurements, and Models*. American Geophysical Union, Washington, DC.

Li, J.-L. F., Waliser, D., Woods, C., Teixeira, J., Bacmeister, J. and co-authors. 2008. Comparisons of satellites liquid water estimates to ECMWF and GMAO analyses, 20th century IPCC AR4 climate simulations, and GCM simulations. *Geophys. Res. Lett.*, **35**, L19710, doi:10.1029/2008GL035427.

Lin, S. J. and Rood, R. B. 1996. Multidimensional flux-form semi-Lagrangian transport schemes. *Mon Wea. Rev* **124**(9), 2046–2070.

Liu, H. Y., Jacob, D. J., Bey, I. and Yantosca, R. M. 2001. Constraints from ^{210}Pb and ^{7}Be on wet deposition and transport in a global three-dimensional chemical tracer model driven by assimilated meteorological fields. *J. Geophys. Res.-Atmos.* **106**(D11), 12109–12128, doi:10.1029/2000JD900839.

Liu, X. and Penner, J. E. 2002. Effect of Mount Pinatubo H_2SO_4/H_2O aerosol on ice nucleation in the upper troposphere using a global chemistry and transport model. *J. Geophys. Res.* **107**(D12), doi:10.1029/2001JD000455.

Liu, X., Penner, J. E. and Herzog, M. 2005. Global modeling of aerosol dynamics: model description, evaluation, and interactions between sulfate and nonsulfate aerosols. *J. Geophys. Res.* **110**, D18206, doi:10.1029/2004JD005674.

Liu, Y. G. and Daum, P. H. 2002. Anthropogenica erosols–Indirect warming effect from dispersion forcing. *Nature* **419**, 580–581.

Lohmann, U. and Feichter, J. 2005. Global indirect aerosol effects: a review. *Atmos. Chem. Phys.* **5**, 715–737.

Mari, C., Jacob, D. J. and Bechtold, P. 2000. Transport and scavenging of soluble gases in a deep convective cloud. *J. Geophys. Res.-Atmos.* **105**(D17), 22255–22267, doi:10.1029/2000JD900211.

Martin, G. M., Johnson, D. W. and Spice, A. 1994. The measurement and parameterization of effective Radius of Droplets in warm stratocumulus clouds. *J. Atmos. Sci.* **51**, 1823–1842.

McFarquhar, G. M. and Heymsfield, A. J. 2001. Parameterizations of INDOEX microphysical measurements and calculations of cloud susceptibility: applications for climate studies. *J. Geophys. Res.-Atmos.* **106**(D22), 28675–28698, doi:10.1029/2000JD900777.

Meskhidze, N., Nenes, A., Conant, W. C. and Seinfeld, J. H. 2005. Evaluation of a new cloud droplet activation parameterization with in situ data from CRYSTAL-FACE and CSTRIPE. *J. Geophys. Res.-Atmos.* **110**, D03301, doi:10.1029/2004JD005082.

Miles, N. L., Verlinde, J. and Clothiaux, E. E. 2000. Cloud droplet size distributions in low-level stratiform clouds. *J. Atmos. Sci.* **57**, 295–311.

Minnis, P., Young, D. F., Sun-Mack, S., Trepte, Q., Doelling, D. R. and co-authors. 2004. CERES cloud products. In *1st CERES-II Science Team Meeting Proceedings*, NCAR, Boulder, Colorado.

Monahan, E. C., Spiel, D. E. and Davidson, K. L. 1986. *A Model of Marine Aerosol Generation via Whitecaps and Wave Disruption*. D. Reidel, Norwell, MA.

Nakicenovic, N., Alcamo, J., Davis, G., de Vries, B., Fenhann, J. and co-authors.2000. *Emissions Scenarios: A Special Report of Working Group III of the Intergovernmental Panel on Climate Change* (eds Nakicenovic and co-editors). Cambridge Univ. Press, New York.

Nenes, A. and Seinfeld, J. H. 2003. Parameterization of cloud droplet formation in global climate models. *J. Geophys. Res.-Atmos.* **108**(D14), 4415–4428, doi:10.1029/2002JD002911.

O'Dowd, C. D., Facchini, M. C., Cavalli, F., Ceburnis, D., Mircea, M. and co-authors. 2004. Biogenically driven organic contribution to marine aerosol. *Nature* **431**, 676–680.

Pawlowska, H. and Brenguier, J. L. 2003. An observational study of drizzle formation in stratocumulus clouds for general circulation model (GCM) parameterizations. *J. Geophys. Res.* **108**(D15), 8630–8642, doi:10.1029/2002JD002679.

Platnick, S., King, M. D., Ackerman, S. A., Menzel, W. P., Baum, B. A. and co-authors. 2003. The MODIS cloud products: algorithms and examples from Terra. *IEEE T Geosci. Remote* **41**, 2, 459–473.

Quaas, J., Boucher, O., Bellouin, N. and Kinne, S. 2008. Satellite-based estimate of the direct and indirect aerosol climate forcing. *J. Geophys. Res.* **113**, D05204, doi:10.1029/2007JD008962.

Radke, L. F., Hegg, D. A., Lyons, J. H., Brock, C. A., Hobbs, P. V. and co-authors. 1988. *Airborne Measurements on Smoke from Biomass Burning*. A. Deepak, Hampton, VA.

Ramanathan, V., Cess, R. D., Harrison, E. F., Minnis, P., Barkstrom, B. R. and co-authors. 1989. Cloud-radiative forcing and climate–results from the earth radiation budget experiment. *Science* **243**, 57–63.

Ramanathan, V., Crutzen, P. J., Lelieveld, J., Mitra, A. P., Althausen, D. and co-authors 2001. Indian Ocean Experiment: an integrated analysis of the climate forcing and effects of the great Indo-Asian haze. *J. Geophys. Res.-Atmos.* **106**(D22), 28371–28398, doi:10.1029/2001JD900133.

Ramanathan, V., Li, F., Ramana, M. V., Praveen, P. S., Kim, D. and co-authors 2007. Atmospheric brown clouds: hemispherical and regional variations in long range transport, absorption, and radiative forcing. *J. Geophys. Res.*, **112**, D22S21, doi:10.1029/2006JD008124.

Reid, S. J., Hobbs, P. V., Rangno, A. L. and Hegg, D. A. 1999. Relationship between cloud droplet effective radius, liquid water content, and droplet concentration for warm clouds in Brazil embedded in biomass smoke. *J. Geophys. Sci.* **D104**, 6145–6153.

Roberts, G., Mauger, G., Hadley, O. and Ramanathan, V. 2006. North American and Asian aerosols over the eastern Pacific Ocean and their role in regulating cloud condensation nuclei. *J. Geophys. Res.-Atmos.* **111**, D13, doi:10.1029/2005JD006661.

Rogers, R. R. and Yau, M. K. 1989. *A Short Course in Cloud Physics*, 3rd Edition, Pergamon Press, Oxford, New York.

Rotman, D. A., Atherton, C. S., Bergmann, D. J., Cameron-Smith, P. J., Chuang, C. C. and co-authors. 2004. IMPACT, the LLNL 3-D global atmospheric chemical transport model for the combined troposphere and stratosphere: model description and analysis of ozone and other trace gases. *J. Geophys. Res.* **109**, D04303, doi:10.1029/2002JD003155.

Rotstayn, L. D. and Liu, Y. G. 2003. Sensitivity of the first indirect aerosol effect to an increase of cloud droplet spectral dispersion with droplet number concentration. *J. Clim.* **16**, 3476–3481.

Schwartz, S. E., Harshvardhan and Benkovitz, C. M. 2002. Influence of anthropogenic aerosol on cloud optical depth and albedo shown by satellite measurements and chemical transport modeling. *Proc. Natl. Acad. Sci. U.S.A.* **99**, 1784–1789.

Stephens, G. L., Vane, D. G., Tanelli, S., Im, E., Durden, S. and co-authors. 2008. CloudSat mission: performance and early science after the first year of operation. *J. Geophys. Res.*, **113**, D00A18, doi:10.1029/2008JD009982.

Turner, D. D., Vogelmann, A. M., Austin, R. T., Barnard, J. C., Cady-Pereira, K. and co-authors. 2007. Thin liquid water clouds—their importance and our challenge. *B. Am. Meteorol. Soc.* **88**, 177–190.

Twomey, S. 1959. The nuclei of natural cloud formation. Part II: the supersaturation in natural clouds and the variation of cloud droplet concentrations. *Geofis. Pure Appl.* **43**, 227–242.

Twomey, S. 1974. Pollution and planetary albedo. *Atmos. Environ.* **8**, 1251–1256.

Uppala, S. M., Kallberg, P. W., Simmons, A. J., Andrae, U., Bechtold, V. D. and co-authors. 2005. The ERA-40 re-analysis. *Q. J. R. Meteorol. Soc.* **131**, 2961–3012.

Wentz, F. J. 1997. A well-calibrated ocean algorithm for special sensor microwave/imager. *J. Geophys. Res.-Oceans* **102**(C4), 8703–8718.

Wilcox, E. M., Roberts, G. and Ramanathan, V. 2006. Influence of aerosols on the shortwave cloud radiative forcing from North Pacific oceanic clouds: results from the Cloud Indirect Forcing Experiment (CIFEX). *Geophys. Res. Lett.* **33**, L21804, doi:10.1029/2006GL027150.

Zhang, L. M., Gong, S. L., Padro, J. and Barrie, L. 2001. A size-segregated particle dry deposition scheme for an atmospheric aerosol module. *Atmos. Environ.* **35**, 549–560.

Zhang, M. H., Lin, W. Y., Klein, S. A., Bacmeister, J. T., Bony, S. and co-authors. 2005. Comparing clouds and their seasonal variations in 10 atmospheric general circulation models with satellite mearurements. *J. Geophys. Res.* **110**, D15S02, doi:10.1029/2004JD005021.